Structure and electric properties of cerium substituted $SrBi_{1.8}Ce_{0.2}Nb_2O_9$ and $SrBi_{1.8}Ce_{0.2}Ta_2O_9$ ceramics

Mohamed Afqir[1,2,*], Amina Tachafine[2], Didier Fasquelle[2], Mohamed Elaatmani[1], Jean-Claude Carru[2], Abdelouahad Zegzouti[1], Mohamed Daoud[1]

[1]*Laboratoire des Sciences des Matériaux Inorganiques et leurs Applications, Faculté des Sciences Semlalia, Université Cadi Ayyad, Marrakech, Morocco*

[2]*Unité de Dynamique et Structure des Matériaux Moléculaires, Université du Littoral Côte d'Opale, Calais, France*

Abstract

$SrBi_{1.8}Ce_{0.2}Nb_2O_9$ (SBCN) and $SrBi_{1.8}Ce_{0.2}Ta_2O_9$ (SBCT) powders were prepared via solid-state reaction method. X-ray diffraction analysis reveals that the SBCN and SBCT powders have the single phase orthorhombic Aurivillius structure at room temperature. The contribution of Raman scattering and FTIR spectroscopy of these samples were relatively smooth and resemble each other. The calcined powders were uniaxially pressed and sintered at 1250 °C for 8 h to obtaine dense ceramics. Dielectric constant, loss tangent and AC conductivity of the sintered Ce-doped $SrBi_2Nb_2O_9$ and $SrBi_2Ta_2O_9$ ceramics were measured by LCR meter. The Ce-doped SBN (SBCN) ceramics have a higher Curie temperature (T_C) and dielectric constant at T_C (380 °C and ε' ~3510) compared to the Ce-doped SBT (SBCT) ceramics (330 °C and ε' ~115) when measured at 100 Hz. However, the Ce-doped SBT (SBCT) ceramics have lower conductivity and dielectric loss.

Keywords: $SrBi_2Nb_2O_9$, $SrBi_2Ta_2O_9$, Ce-doping, structure, conductivity, dielectric measurments

I. Introduction

Aurivillius phases have been extensively investigated since they were discovered in 1949 by Aurivillius [1]. Among different ceramics with Aurivillius structures, $SrBi_2Nb_2O_9$ and $SrBi_2Ta_2O_9$ are of high importance as a lead-free system due to good dielectric and ferroelectric properties. They belong to a multilayer family of so-called Aurivillius phase with a general chemical formula $(Bi_2O_2)^{2+}(A_{m-1}B_mO_{3m+1})^{2-}$, where A is a combination of one or more mono-, di- and trivalent ions with 12-fold coordinated cation, B is a combination of tetra-, penta-, and hexavalent ions with 6-fold coordinated cation and *m* refers to the number of BO_6 octahedra between neighbouring Bi_2O_2 layers along the c-axis [2]. $SrBi_2Nb_2O_9$ (SBN) and $SrBi_2Ta_2O_9$ (SBT) are attracting interest for their application in ferroelectric random access memories (FeRAM) [3–6].

Boullay *et al.* [7] reported the investigation of the phase transition sequence in $SrBi_2Ta_2O_9$ and $SrBi_2Nb_2O_9$ using single-crystal X-ray diffraction. They showed that by monitoring specific reflections as a function of temperature, sensitive either to the super-structure formation or to polar displacements, it is possible to check the existence of an intermediate phase of two isostructural Aurivillius phases. This latter was confirmed in SBT, but within experimental accuracy could not be detected in SBN. Miura [8] investigated $SrBi_2Nb_2O_9$, $SrBi_2Ta_2O_9$ and $PbBi_2Nb_2O_9$ using a first-principles calculation method with optimized structures. In the optimized structures, the displacement of Ta in TaO_6 octahedra of SBT is small compared to the displacement of Nb in NbO_6 octahedra of SBN which is larger.

Substitution with Ce^{3+} ions plays a significant role in tailoring a desirable structure and appropriate dielctric properties of different ceramic systems. To our knowledge, there is only a few papers [9,10] investigating the

*Corresponding author: +2126 42 37 94 83,
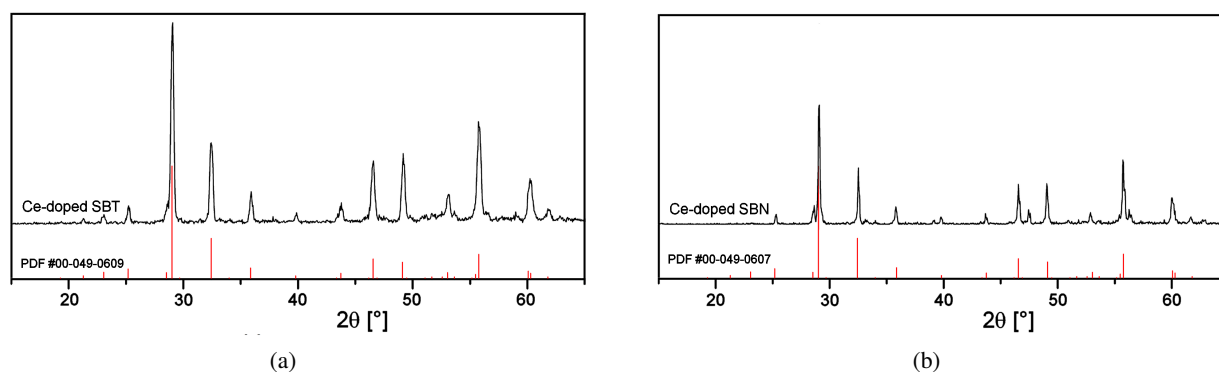e-mail: *mohamed.afqir@yahoo.fr*

Figure 1. XRD patterns of Ce-doped: a) SBT and b) SBN calcined powders

substitution of bismuth by cerium in $SrBi_2Nb_2O_9$ and $SrBi_2Ta_2O_9$. The influence of the cerium substitution in SBN and SBT on structure and properties is of fundamental interest in condensed matter chemicals. For that reason we prepared Ce-doped SBN and Ce-doped SBT by the solid-state method, investigated their structures (X-ray diffraction, FTIR, Raman) and analysed dielectric properties of the sintered ceramics.

II. Experimental

Cerium doped SBN and SBT were prepared by the solid-state reaction method. Stoichiometric amounts of raw materials, Bi_2O_3 (Rectapur, 99%), $SrCO_3$ (Labosi), Ta_2O_5 (Fluka, 99.9%), Ce_2O_3 and Nb_2O_5 (Acros Organics, 99.5%), were intimately ground manually in a mortar for one hour. Excess of Bi_2O_3 (10 wt.%) was introduced to compensate evaporation of Bi_2O_3 during heat treatments. The obtained powders were calcined at 1200 °C during 12 h.

The samples were then uniaxially pressed at 0.5 MPa into pellets having 6 mm in diameter. The pellets were coverd with powders of the same materials and heated at 1250 °C for 8 h. Anchor paste was deposited on both surfaces of the ceramic disc and fired at 200 °C for 1 h to form appropriate electrodes for electrical measurements.

The powders were examined by X-ray diffraction (PANalytical/Philips X'pert) with CuKα radiation to determine phase purity. The samples were also characterized by Raman (Bruker, Vertex 70) and Fourier transform infrared spectroscopy (KBr-pellet/ Bruker, Vertex 70 DTGS). Conductivity and dielectric properties were measured at temperatures ranging from room temperature to 500 °C using an LCR meter HP 4284A (Hewlett Packard Co).

III. Results and discussion

3.1. X-ray diffraction

Figure 1 shows the XRD patterns of the calcined SBCT (Ce-doped SBT) and SBCN (Ce-doped SBN) powders. The patterns of SBCT and SBCN were identified to match with the standard XRD card of $SrBi_2Ta_2O_9$

(PDF #00-049-0609) and $SrBi_2Nb_2O_9$ (PDF #00-049-0607). Both powders show the presence of the pure single Aurivillius phase with an orthorhombic $A2_1am$ space group. The highest peak corresponds to (115) orientation for both samples, which is consistent with the highest diffraction peak in bismuth layered structured ferroelectrics systems [11]. The peak position shifts slightly, indicating that cerium ions have diffused into the crystal lattice formed a solid solution.

The effect of Ce-ions on the crystal structure of SBT and SBN samples is summarized in Table 1. The difference observed in lattice parameters for the same materials may be due to the incorporation of Ce^{3+} ions into the Bi-sites. The radius of Bi^{3+} (0.093 nm) is smaller than that of Ce^{3+} (0.101 nm) [12]. The value of the orthorhombic distortion (b/a) almost retains the same. The tetragonal strain (c/a) decreases significantly for SBCN, but it decreases smoothly for SBCT powder.

Table 1. Lattice parameters of pure and doped SBT and SBN

	SBT	Ce-doped SBT	SBN	Ce-doped SBN
a [Å]	5.554	5.533	5.519	5.518
b [Å]	5.551	5.529	5.515	5.512
c [Å]	25.144	25.030	25.112	25.073
c/a	4.527	4.524	4.838	4.543
b/a	0.999	0.999	0.999	0.998

3.2. FTIR and Raman measurements

Figure 2 illustrates the Raman spectra of the calcined SBCT (cerium doped SBT) and SBCN (cerium doped SBN) powders. The band at 89 cm⁻¹ appeared may be due to the A_{1g} mode, involving the vibrations of Sr atoms. The A_{1g} mode is due to the heavy atom vibrations at 89 cm⁻¹ (Sr) and 140 cm⁻¹ (Bi). The peak at 172 cm⁻¹ and 164 cm⁻¹ originates from vibration in *a–b* plane of Nb and Ta, respectively [13]. The band at 210 cm⁻¹ for both samples represents the mode A_{1g} of Sr–O with a rock salt structure. The bands at 567 (for SBCN) and 600 cm⁻¹ (for SBCT) can be assigned to the vibrations of oxygen atoms in the Bi–O planes. Whereas the A_{1g} mode is attributable to the vibration of the O3 oxygen atom in Bi–O plane [14]. The modes at 812 cm⁻¹
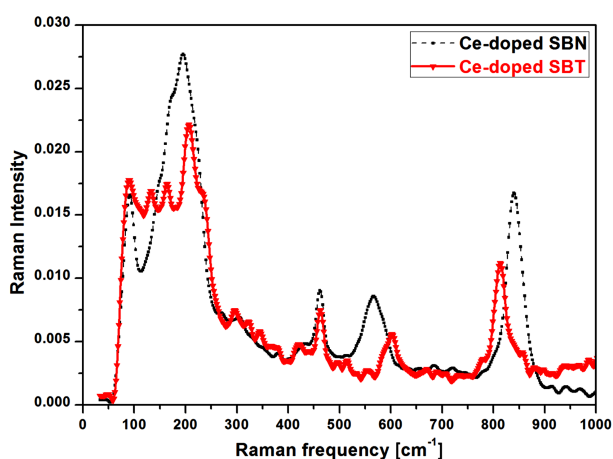
Figure 2. Raman spectra of SBCT and SBCN powders

Figure 3. FTIR spectra of SBCT and SBCN powders

and 835 cm^{-1} reflect the stretching mode of TaO$_6$ and NbO$_6$ [15], respectively. The observed shift is due to a large difference in the atomic mass of Nb (92.90 g/mol) and Ta (180.94 g/mol) and may be ascribed to the binding strength (Nb–O; 753 kJ/mol and Ta–O; 805 kJ/mol). Note that the displacement of Nb in NbO$_6$ octahedra in SBN is much larger than that of Ta in TaO$_6$ octahedra in SBT. This mode is associated with E_g modes related to the stretching of oxygen bonds in the octahedron [16].

The infrared spectra of the calcined SBCT and SBCN powders were obtained from transmission data and can be found in Fig. 3. Three observed absorption bands, at around 426 cm^{-1} (SBCT) and 432 cm^{-1} (SBCN); 640 cm^{-1} (SBCT) and 615 cm^{-1} (SBCN); 788 cm^{-1} (SBCT) and 808 cm^{-1} (SBCN), are in good agreement with the reported data [17]. The strongest bands at 640 cm^{-1} and 615 cm^{-1} are assigned to Nb–O and Ta–O stretching vibration, respectively. The weakest bands at 426 cm^{-1} and 432 cm^{-1} are assigned to Nb–O and Ta–O bending vibration, respectively. The bands at 788 cm^{-1} and 808 cm^{-1} are assigned to the vibrations arising from the strangely covalently bonded $(Bi_2O_2)^{2+}$ layers. The spectra show also a band at 550 cm^{-1} for

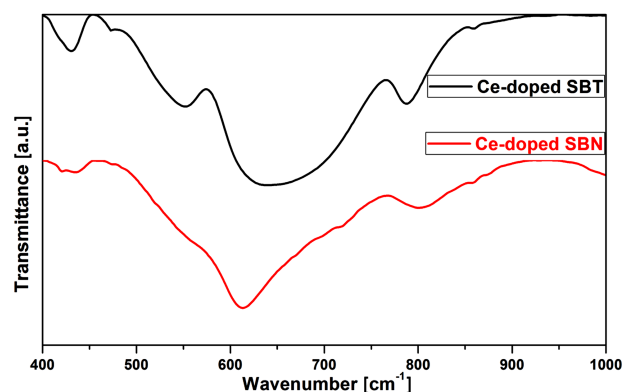SBCT which was found to be sharper for SBCN sample, these bands are related to Ce–O vibration bonds [18].

It is found that FTIR and Raman spectra of these species show a strong resemblance. The effect of Ce substitution does not bring significant change in the structure.

3.3. Dielectric measurements

Figure 4 illustrates the frequency dependence of dielectric constant (ε') and dielectric loss ($\tan\delta$) at room temperature of the sintered Ce-doped SBT (SBCT) and Ce-doped SBN (SBCN) ceramics. The room temperature dielectric constant of the SBCN ceramics decreases with frequency from ~1000 at 1 kHz to ~20 at 1 MHz, whereas ε' is almost constant (~100) for the investigated frequencies in the case of the SBCT ceramics. It is also evident that, in the studied frequency range, there is no significant change in the dielectric loss (which are relatively low) of the SBCT sample, but the variation is more pronounced for the SBCN ceramics (Fig. 4).

Figure 5 shows the temperature dependence of the dielectric constant (ε') and dielectric loss ($\tan\delta$) at 100 Hz and 1 kHz. The broad peak of dielectric constant at 100 Hz, corresponding to the Curie temperature T_C, can be seen at 380 °C and 326 °C for the SBCN and SBCT
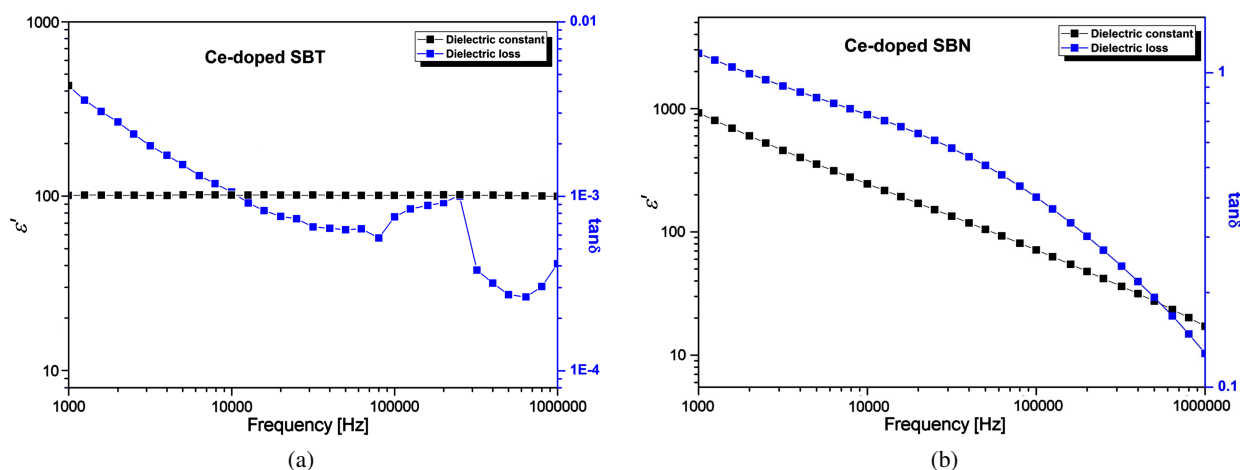

Figure 4. Frequency dependence of dielectric constant and dielectric loss of: a) SBCT and b) SBCN ceramics at room temperature
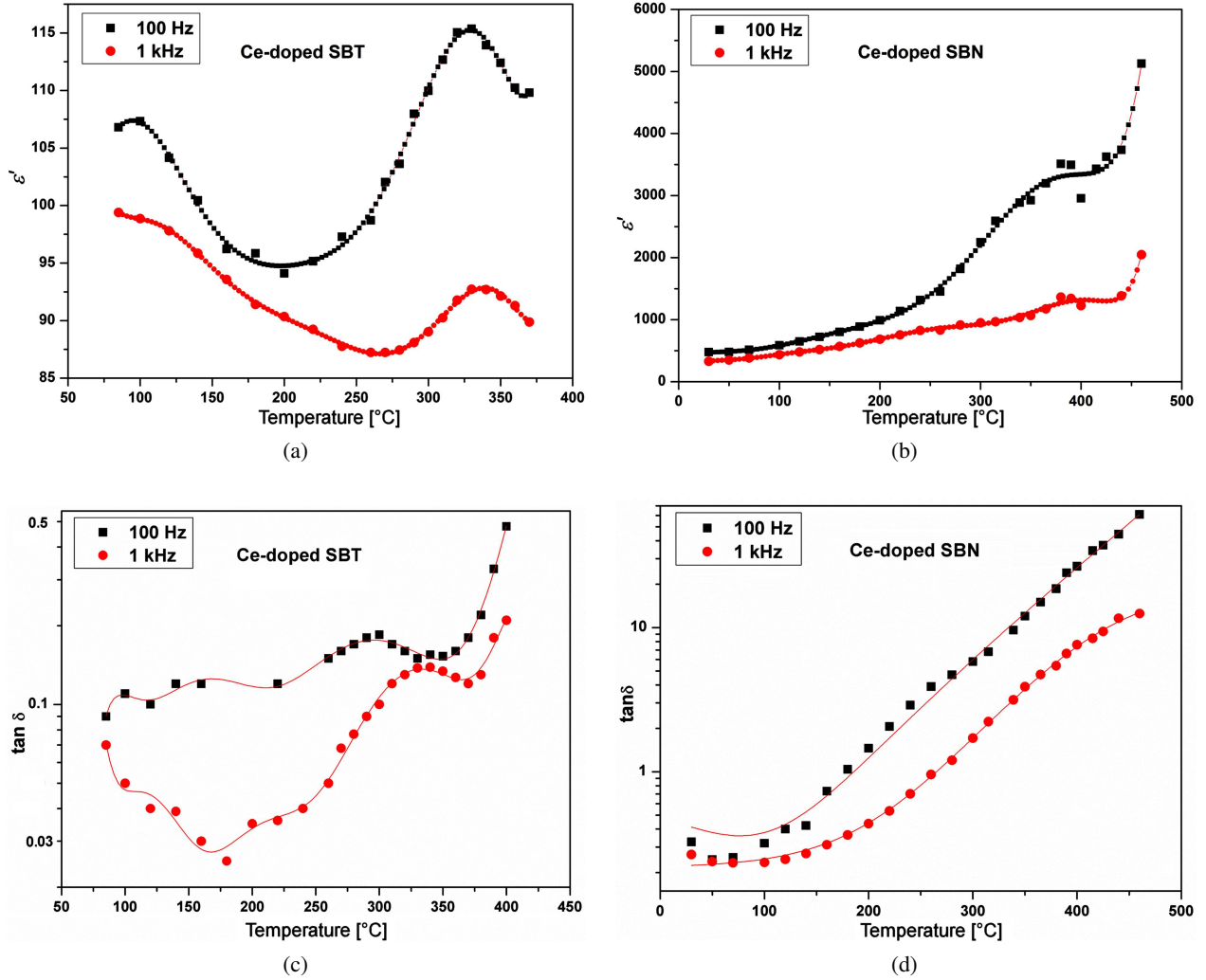
Figure 5. Temperature dependence of dielectric constant, ε' (a,b) and dielectric loss, tan δ (c,d) of SBCN and SBCT ceramics

ceramics, respectively. These values are close to the values which can be found in literture, i.e. ~440 °C for SrBi$_2$Nb$_2$O$_9$ and ~335 °C for SrBi$_2$Ta$_2$O$_9$ [19–21]. The fact that orbital hybridization of Ta–O bands is weaker than that of Nb–O is the reason for the difference in T_C between tantalates and niobates [22]. In addition, the observed difference between T_C in the pure and Ce-doped SBN/SBT ceramics is due to the lattice distortion and presence of Ce ions. This tendency was already confirmed by other authors [10], which showed that the substitution of cerium ions onto the sites of bismuth in bismuth layer-structured ferroelectric (BLSF) leads to decrease T_C.

Dielectric constant at T_C and 100 Hz was found to be 3510 and 115 for the sintered SBCN and SBCT samples, respectively. This could be due to the large difference between the ionic polarizabilities of Nb^{5+} (0.242 Å^3) and Ta^{5+} (0.185 Å^3).

The dielectric loss measured at 100 Hz for the sintered SBCN ceramics increases steeply with temperature from ~1.5 at 200 °C to ~26 at 400 °C. However, much lower values of tan δ are characteristic of the SBCT ceramics.

3.4. Conductivity measurements

The conductivity of the sintered SBCT and SBCN ceramics as a function of temperature at 100 Hz are plotted in Fig. 6. Conductivity was calculated by:

$$\sigma = \omega \cdot \varepsilon_0 \cdot \varepsilon' \cdot \tan \delta \tag{1}$$

and the activation energy (E_a) for the conductivity was determined from the Arrhenius equation given by:

$$\sigma = \sigma_0 \cdot \exp\left(\frac{-E_a}{k_B T}\right) \tag{2}$$

where ω is the angular frequency, ε_0 is the dielectric constant in free space, σ_0 is a constant, E_a is the activation energy, k_B is the Boltzmann's constant and T is temperature. The Ce-doped SBT (SBCT) ceramics has low conductivity and relatively complex behaviour (Fig. 6a). On the other hand, the conductivity of the Ce-doped SBN (SBCN) ceramics increases with an increase in temperature (Fig. 6b). At low temperatures conductivity is dominated by mobility of extrinsic defects. However, at high temperatures conductivity is due to thermally formed (intrinsic) defects. The room temperature
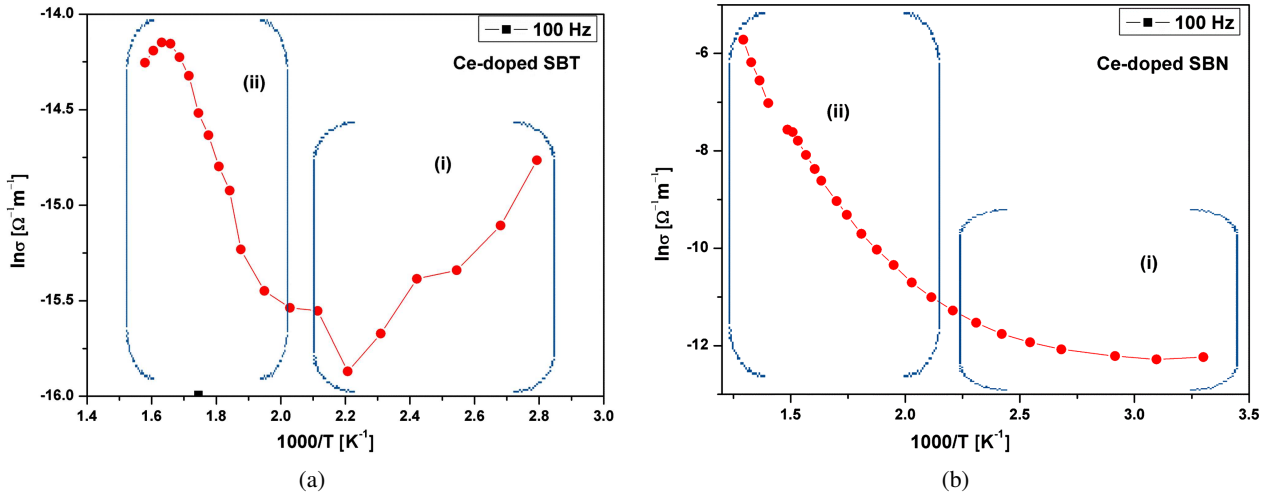
Figure 6. Arrhenius plots of: a) SBCT and b) SBCN ceramics

resistivity of the SBCN sample varies in the order of 10^{10} to 10^{12} Ωcm. At high temperatures it is due to the thermally activated oxygen vacancies [23]. The activation energy estimated from 2.2 K^{-1} (181 °C) to 1.5 K^{-1} (393 °C) is found to be 0.51 eV and 0.41 eV for the SBCN and SBCT samples, respectively.

The ionization of oxygen vacancies can be described by Kroger-Vink notation. Excess oxygen vacancies and electrons are formed through the reduction reaction:

$$O_O^x \longrightarrow \tfrac{1}{2} O_2(\uparrow) + V_O^{\bullet\bullet} + 2\,e' \tag{3}$$

Thus, the generation of oxygen vacancies and electrons, leads to a rise in conductivity by the hopping mechanism between the available sites. The presence of Ce^{3+} in the lattice may also reduce the oxygen vacancy formation. The bond dissociation energy of Ce–O (353 kJ/mol) is larger than that of Bi–O (343 kJ/mol) [24]. Hence, the substitution of Bi by Ce suppresses the formation of oxygen vacancies.

In the light of the above mentioned, the Ce-doped SBN (SBCN) ceramics show the high value of T_C, but suffer from high dielectric loss and low dielectric constant at room temperature. On the other hand the Ce-doped SBT (SBCT) ceramics show dielectric properties at room temperature, which are desirable in nonvolatile FeRAM applications.

IV. Conclusions

In this paper synthesis of $SrBi_{1.8}Ce_{0.2}Nb_2O_9$ (SBCN) and $SrBi_{1.8}Ce_{0.2}Ta_2O_9$ (SBCT) powders by solid-state reaction method and sintering of uniaxially pressed pellets were presented. XRD patterns showed the presence of the parent ($SrBi_2Nb_2O_9$, $SrBi_2Ta_2O_9$) phase without any secondary phase. Raman and FTIR studies for both samples, show that the spectra comprise identical nature, suggesting that the incorporation of Ce^{3+} in SBN and SBT systems does not bring significant change in the structure. Dielectric measurements showed that the

Ce-doped SBN ceramics have a higher Curie temperature (T_C) and dielectric constant at T_C (380 °C and ε' ~3510) compared to the Ce-doped SBT ceramics (330 °C and ε' ~115) when measured at 100 Hz. However, the Ce-doped SBT ceramics have lower conductivity and dielectric loss.

References

1. B. Aurivillius, "Mixed bismuth oxides with layered lattices: Structure type of $CaBi_2B_2O_9$", *Arkiv. Kemi*, **1** (1949) 463–480.
2. T. Badapanda, R.K. Harichandan, S.S. Nayak, A. Mishra, S. Anwar, "Frequency and temperature dependence behaviour of impedance, modulus and conductivity of $BaBi_4Ti_4O_{15}$ Aurivillius ceramic", *Process. Appl. Ceram.*, **8** (2014) 145–153.
3. D. Kajewski, Z. Ujma, "Electrical properties of $SrBi_2(Nb_{0.5}Ta_{0.5})_2O_9$ ceramics", *J. Phys. Chem. Solids*, **71** (2010) 24–29.
4. P. Duran-Martin, A. Castro, P. Millan, B. Jimenez, "Influence of Bi-site substitution on the ferroelectricity of the Aurivillius compound $Bi_2SrNb_2O_9$", *J. Mater. Res.*, **13** (1998) 2565–2571.
5. V.V. Sidsky, A.V. Semchenko, A.G. Rybakov, V.V. Kolos, A.S. Turtsevich, A.N. Asadchyi, W. Strek, "La^{3+}-doped $SrBi_2Ta_2O_9$ thin films for FRAM synthesized by sol-gel method", *J. Rare Earth*, **32** (2014) 277–281.
6. T. Eshita, T. Tamura, Y. Arimoto, "Ferroelectric random access memory (FRAM) devices", pp. 434–454 in *Advances in Non-Volatile Memory and Storage Technology*. Ed. Y. Nishi, Elesevier Ltd., 2014.
7. P. Boullay, J. Tellier, D. Mercurio, M. Manier, F.J. Zuñiga, J.M. Perez-Mato, "Phase transition sequence in ferroelectric Aurivillius compounds investigated by single crystal X-ray diffraction", *Solid State Sci.*, **14** (2012) 1367–1371.
8. K. Miura, "Electronic and structal properties of ferroelectric $SrBi_2Ta_2O_9$, $SrBi_2Nb_2O_9$ and

PbBi$_2$Nb$_2$O$_9$", *J. Korean Phys. Soc.*, **42** (2003) S1244–S1247.

9. P. Fang, Z. Xi, W. Long, X. Li, J. Li, "Structure and electrical properties of SrBi$_2$Nb$_2$O$_9$-based ferroelectric ceramics with lithium and cerium modification", *J. Alloys Compd.*, **575** (2013) 61–64.

10. V. Senthi, T. Badapand, A. Chandrabos, S. Panigrahi, "Dielectric and ferroelectric behaviour of cerium modified SrBi$_2$Ta$_2$O$_9$ ceramic", *Mater. Lett.*, **159** (2015) 138–141.

11. C.L. Diao, J.B. Xu, H.W. Zheng, L. Fang, Y.Z. Gu, W.F. Zhang, "Dielectric and piezoelectric properties of cerium modified BaBi$_4$Ti$_4$O$_{15}$ ceramics", *Ceram. Int.*, **39** (2013) 6991–6995.

12. N. Pavlović, D. Kancko, K. Mészáros Szécsényi, V.V. Srdić, "Synthesis and characterization of Ce and La modified bismuth titanate", *Process. Appl. Ceram.*, **3** (2009) 88–95.

13. J. Qiu, G.-Z. Liu, M. He, H.-S. Gu, T.-S. Zhou, "W doping-dependent structural and ferroelectric properties of SrBi$_2$Nb$_2$O$_9$ ferroelectric ceramics", *Physica B.*, **400** (2007) 134–136.

14. R. Singh, V. Luthra, Archana, R.P. Tandon, "Structural, dielectric and piezoelectric properties of SrBi$_2$Nb$_2$O$_9$ and Sr$_{0.8}$Bi$_{2.2}$Nb$_2$O$_9$ ceramics", *Ceram. Int.*, **41** (2015) 4468–4478.

15. J.S. Zhu, H.X. Qin, Z.H. Bao, Y.N. Wang, W.Y. Cai, P.P. Chen, W. Lu, H.L. W. Chan, C.L. Choy, "X-ray diffraction and Raman scattering study of SrBi$_2$Ta$_2$O$_9$ ceramics and thin films with Bi$_3$TiNbO$_9$ addition", *Appl. Phys. Lett.*, **79** (2001) 3827.

16. M.J.S. Rocha, M.C.C. Filho, K.R.B. Theophilo, J.C. Denardin, I.F. Vasconcelos, E.B. Araujo, A.S.B. Sombra, "Ferrimagnetism and ferroelectricity of the composite matrix: SrBi$_2$Nb$_2$O$_9$(SBN)$_X$-BaFe$_{12}$O$_{19}$(BFO)$_{100-X}$", *Mater. Sci. Appl.*, **3** (2012) 6–17.

17. M. Verma, A. Tanwar, K. Sereenivas, V. Gupta, "Dielectric and ferroelectric properties of SrBi$_2$Nb$_2$O$_9$ and SrBi$_{1.9}$La$_{0.1}$Nb$_2$O$_9$ ceramics", *Ferroelctrics*, **404** (2010) 233–239.

18. R. Suresh, V. Ponnuswamy, R. Mariappan, "Effect of annealing temperature on the microstructural, optical and electrical properties of CeO$_2$ nanoparticles by chemical precipitation method", *Appl. Surf. Sci.*, **273** (2013) 457–464.

19. V.A. Isupov, "Two types of ABi$_2$B$_2$O$_9$ layered perovskite-like ferroelectrics", *Inorg. Mater.*, **43** (2007) 976–979.

20. A. Onodera, M. Fukunaga, M. Takesada, "Ferroelectric instability and dimensionality in Bi-layered perovskites and thin films", *Adv. Condensed Matter Phys.*, **2012** (2012) 714625.

21. J.-H. Ko, A. Hushur, S. Kojima, B.C. Sih, Z.-G. Ye, "Acoustic anomalies and central peak in SrBi$_2$Ta$_2$O$_9$ single crystals studied by micro-Brillouin scattering", *Appl. Phys. Lett.*, **81** (2002) 4043.

22. Zulhadjri, B. Prijamboedi, A.A. Nugroho, N. Mufti, A. Fajar, T.T.M. Palstra, Ismunandar, "Aurivillius phases of PbBi$_4$Ti$_4$O$_{15}$ doped with Mn^{3+} synthesized by molten salt technique: Structure, dielectric, and magnetic properties", *J. Solid State Chem.*, **184** (2011) 1318–1323.

23. M. Raghavender, G.S. Kumar, G. Prasad, "Electrical properties of La-modified strontium bismuth titanate", *Indian J. Pure Appl. Phys.*, **44** (2006) 46–51.

24. T.L. Cottrell, *The Strengths of Chemical Bonds*, 2nd ed., Butterworth, London, 1958.